PHYSICAL REVIEW B **93**, 220402(R) (2016)

Nanometer-scale exchange interactions between spin centers in diamond

V. R. Kortan, C. Şahin, and M. E. Flatté
Optical Science and Technology Center and Department of Physics and Astronomy, University of Iowa, Iowa City, Iowa 52242, USA
(Received 10 March 2016; revised manuscript received 22 May 2016; published 15 June 2016)

Exchange interactions between isolated pairs of spin centers in diamond have been calculated, based on an accurate atomistic electronic structure for diamond and any impurity atoms, for spin-center separations of up to 2 nm. The exchange interactions exceed dipolar interactions for spin-center separations of less than 3 nm. NV^- spin centers, which involve two lattice sites which differ from the host, interact very differently depending on the relative orientations of the symmetry axis of the spin center and the radius vector connecting the pair. Exchange interactions between transition-metal dopants behave similarly to those of NV^- centers. The Mn-Mn exchange interaction decays with a much longer length scale than the Cr-Cr and Ni-Ni exchange interactions, exceeding dipolar interactions for Mn-Mn separations of less than 5 nm. Calculations of these highly anisotropic and spin-center-dependent interactions provide the potential for the design of spin-spin interactions for novel nanomagnetic structures.

DOI: 10.1103/PhysRevB.93.220402

A single spin, such as from a defect or dopant, can control the properties of a nanomagnetic system [1], suggesting pathways to constructing novel magnetic materials or magnetic behavior through designed assembly, e.g., of spins in metals, insulators, and semiconductors [2–8]. Many spin centers in wide-gap semiconductors such as diamond exhibit exceptionally long room-temperature spin coherence times [9], permitting coherent interactions among such spin centers over length scales of many nanometers, and the corresponding shaping of spin dynamics in the spin assemblies. As the interactions occur through weak, long-range, largely isotropic dipolar interactions [10,11], the interaction effects on spin dynamics are slow (less than 1 μeV). Continued improvement of control in spin-center positioning, such as through ion implantation [4,12,13], will lead to assemblies with short-range coupling, where exchange interactions may dominate over dipolar interactions, producing anisotropic [3] interactions that are orders of magnitude greater than dipolar interactions. The current focus on NV^- centers in diamond, due especially to the convenience of its levels and optical selection rules for spin initialization and readout [14], may also shift to other spin centers that are easier to address and manipulate electrically, especially transition-metal dopants that possess partially filled d levels [15,16].

Here, we construct a highly accurate theoretical description of the spin center in bulk diamond, and a very efficient theoretical methodology to evaluate the exchange coupling between spins in diamond, including both NV^- centers and transition-metal spin centers. We include the weak spin-orbit interaction in bulk diamond and the strong spin-orbit interaction of a transition-metal dopant, as well as the dependence of an NV^- spin center's interaction on the N-V axis direction. We find that exchange interactions dominate over dipolar interactions for spin-center separations smaller than 3 nm, except for the more delocalized Mn spins, which are exchange dominated for separations of less than 5 nm. The theoretical techniques that have been previously applied to diamond find calculations of spin-spin interactions very challenging, either (as with density functional theory [15–17]) due to the very large supercell sizes required for such calculations, or (as with symmetry-based group-theory analyses [18]) due to the inability to constrain the problem to a very small number of experimentally determined quantities. Our approach is a rigorously tested $spds^*$ description of the bulk electronic structure [19] and a set of effective impurity potentials, including for d states, that replicates the energies of the spin-center states found in density functional theory calculations or experimental measurements. Once those are known, the electronic properties of the pair are efficiently evaluated using a Green's function-based Koster-Slater method [20] as described in Ref. [21], and here extended to the $spds^*$ system required to accurately describe bulk diamond and the d levels of transition-metal dopants. The exchange energies typically change less than 10% for a change in the defect energy of 100 meV, indicating that these results are determined mostly by the previously characterized accuracy of the host electronic structure and are less sensitive to errors in the midgap state energies of the dopants. This approach [21], by exactly solving for the electron propagator in the regions between defects, permits calculations of the exchange interaction of a defect pair to proceed with a rapid speed that is independent of the defect separation. For these pair calculations, typical calculations of the exchange interaction for a defect pair configuration take between 1 and 10 min on a current laptop computer for the accuracies presented here, whereas the full calculation of the propagator between two atomic sites for a range of energies including the band gap and a broadening of 100 meV takes approximately ten minutes on the same laptop computer.

The Hamiltonian for a point defect (impurity atom or vacancy) has the form $H = H_0 + V$, where H_0 is the $spds^*$ Hamiltonian of Ref. [19] and

$$\begin{aligned} V = & \sum_{\ell,m,s} U^{os}_{\ell ms} c^{\dagger}_{\ell ms}(\mathbf{R_0}) c_{\ell ms}(\mathbf{R_0}) \\ & + \sum_{j=1}^{4} \sum_{\ell} U^{nn}_{\ell ms} c^{\dagger}_{\ell ms}(\mathbf{R_j}) c_{\ell ms}(\mathbf{R_j}) \\ & + (2/3) \sum_{\ell,m,s} \Delta_{\ell} [c^{\dagger}_{\ell ms}(\mathbf{R_0}) c_{\ell m+1 s-1}(\mathbf{R_0}) + \text{H.c.}]. \quad (1) \end{aligned}$$

Here, $U_{\ell ms}$ is the energy difference for the orbital with spin s, angular momentum ℓ, and azimuthal quantum number m,

TABLE I. On-site potentials (eV) for transition-metal impurities in diamond, including the nonmagnetic and magnetic potentials for d electrons of t_2 and e symmetry, and the spin-orbit interaction strength Δ for p and d electrons, in eV.

	Nonmagnetic		Magnetic		Spin orbit	
	t_2	e	t_2	e	p	d
Cr	− 18.89	− 21.45	− 0.26	− 1.85	0.09	0.02
Mn	− 19.30	− 22.50	− 0.14	− 1.00	− 0.03	− 0.08
Fe	− 19.20	− 23.15	0	0	− 0.15	− 0.12
Co	− 20.57	− 24.64	− 0.26	− 0.21	− 0.10	− 0.19
Ni	− 21.67	− 27.03	− 0.43	− 0.38	− 0.08	− 0.33

either at the point defect site (U^{os}) or at the nearest neighbors (U^{nn}), and Δ_ℓ is the point defect's spin-orbit interaction for the ℓ angular-momentum states. $c^\dagger_{\ell ms}(\mathbf{R})$ [$c_{\ell ms}(\mathbf{R})$] is the creation (annihilation) operator for a spin-s electron in the ℓ,m orbital at site $\mathbf{R}$. The point defect is located at $\mathbf{R_0}$, and the four nearest-neighbor sites are labeled by $\mathbf{R_1}$–$\mathbf{R_4}$. The spin-orbit potential has been calculated from atomic energies [22–24] using the Landé interval rule. Spin-orbit interactions are positive for angular-momentum shells less than half full, and negative otherwise. For transition-metal dopants, to position the d states of correct tetrahedral symmetry (t_2 or e) at the correct locations within the diamond band gap (determined from *ab initio* calculations [16]), U^{os} magnetic and nonmagnetic potentials are determined for the t_2 and e states, and reported in Table I. $U^{nn} = 0$ for transition-metal dopants. For the NV^- spin center, defect potentials are only required on the p orbitals, however, the shift in the atomic positions requires nonzero defect potentials on the nearest neighbors as well. These values are reported in Table II.

We calculate the retarded Green's function for the bulk Hamiltonian H_0, $G_0(\mathbf{k},\omega) = [\omega - H_0(\mathbf{k}) + i\delta]^{-1}$, and from this the real-space Green's function $G_0(\mathbf{R_i},\mathbf{R_j},\omega)$, where G_0 is a matrix with rows and columns labeled by ℓ, m, and s. The properties of the defects, either point defects or pairs, are determined from solving the Dyson equation in real space,

$$G(\omega) = [I - G_0(\omega)V]^{-1}G_0(\omega). \tag{2}$$

Due to the limited number of positions in real space where the potential is nonzero, Eq. (2) can be solved rapidly once the $G_0(\mathbf{R_i},\mathbf{R_j},\omega)$ have been tabulated.

Figure 1 compares the on-site and nearest-neighbor spin-resolved local density of states (LDOS) for the two transition-metal spin-1 dopants, Ni and Cr. Within the diamond band gap, the Cr spin center forms one doubly degenerate spin-up and one doubly degenerate spin-down e level as well as one triply degenerate spin-up and one triply degenerate spin-down t_2 level. The ground state for Cr has two electrons in the spin-up e state and the rest empty. The Ni dopant levels are arranged differently, with the t_2 levels in the gap and the e levels below the edge of the valence band, showing as a broad resonance. The t_2 levels for Ni show a visible splitting in Fig. 1 due to the large spin-orbit coupling for Ni. The ground state for the Ni spin center has two electrons in the spin-up t_2 states. As found in Refs. [15,16] with density functional theory calculations, the Cr ground state possesses more spectral weight on the site of the dopant than the Ni ground state, with a ratio of ∼2:1. The construction of the NV^- center requires tracking different midgap levels. The NV^- center exhibits four levels in the gap, the lower two having a_1 symmetry and the upper two are spin-split, orbitally degenerate e_x and e_y levels, all of which originate from p orbitals (t_2 character) [17]. The ground state for the NV^- center fills electrons up through the spin-up e_x and e_y states.

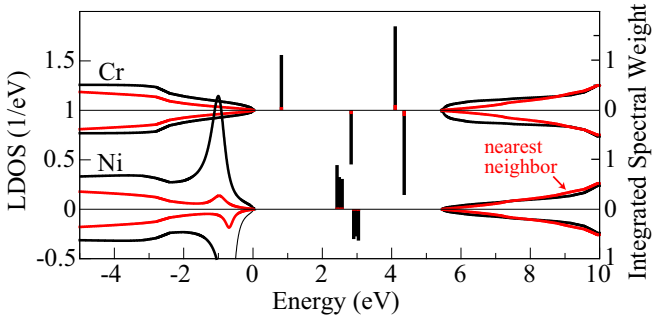

FIG. 1. Spin-resolved local density of states (LDOS) on the impurity site and nearest-neighbor carbon site for Cr and Ni spin centers. The continuum states in the conduction and valence bands are plotted on the scale of the left axis. The probabilities of finding the electron on the impurity for midgap impurity states are plotted on the scale of the left axis. The nearest-neighbor contributions are in red, whereas the on-site contributions are in black.

TABLE II. On-site and nearest-neighbor p-orbital potentials, magnetic and nonmagnetic, for nitrogen and a vacancy in diamond.

	On site		Nearest neighbor	
	Nonmagnetic	Magnetic	Nonmagnetic	Magnetic
N	−5.33	2.93	0	0
V	50	0	−0.26	−2.97

These trends are reflected in the real-space probability density of the highest occupied molecular orbital (HOMO) of each of the spin centers in Fig. 2. The ground state spins for each dopant in diamond are Fe: spin 0; Mn and Co: spin $\frac{1}{2}$; and NV^-, Cr, and Ni: spin 1. All of the transition-metal dopant HOMOs show the same overall spatial symmetry regardless of spin, which is expected because the propagation of electron waves in the host material most determines the probability density symmetry [21]. The Fe, Mn, and Cr dopants all have e-like HOMOs whereas the NV^-, Co, and Ni spin centers have t_2-like HOMOs, and therefore among the point defects, Fe, Mn, and Cr all have a larger wave function probability near the dopant location and appear less extended than the Co and Ni wave functions.

Once the properties of an individual spin center have been determined, the exchange interaction between two can be calculated by comparing the energies of filled midgap states for parallel and antiparallel alignment of the spin centers [3,21]. The exchange interaction found between pairs of transition-metal spin centers is shown in Fig. 3. For pairs spaced along the $[1\bar{1}0]$ direction, the Mn-Mn pair has the largest and slowest-decaying exchange, followed by Cr-Cr pairs, and then

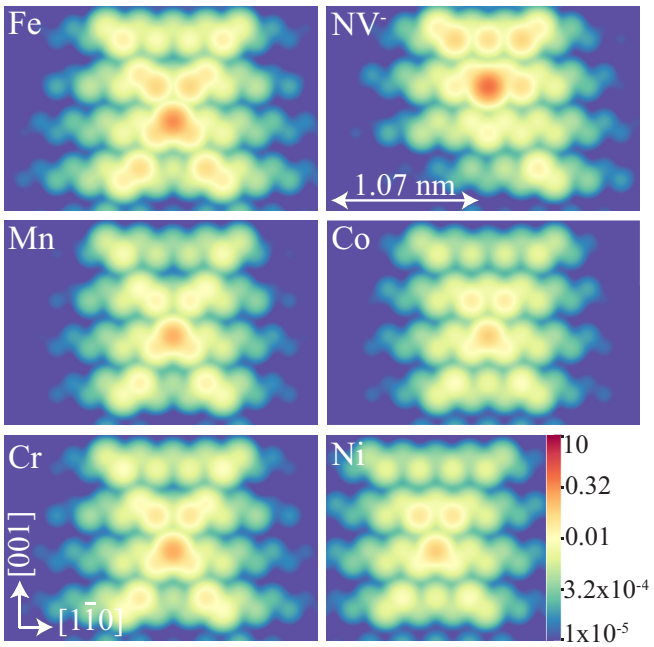

FIG. 2. Real-space probability density for (a) Fe, (b) NV^-, (c) Mn, (d) Co, (e) Cr, and (f) Ni dopants with any background contribution from the homogeneous diamond crystal removed. The slices are taken in the (110) plane and three atomic layers above the dopant. The logarithmic color scale for all plots is the same, and is in units of the inverse volume of an atomic site.

Ni-Ni pairs. Pair calculations are performed by introducing two copies of the potential in Eq. (1) at the two locations of the dopants. The response of the molecular midgap states yields the exchange interaction. The exchange interaction between Cr and Ni appears often smaller than either the Cr-Cr or Ni-Ni exchange, which is likely due to the smaller hybridizations of the energy levels of Cr and Ni (relative to homodopant pairs) due to their different energies. Along the [001] direction the Ni-Ni pair does not decrease logarithmically for the closest pair spacings. The exchange interaction along the [1$\bar{1}$1] interaction

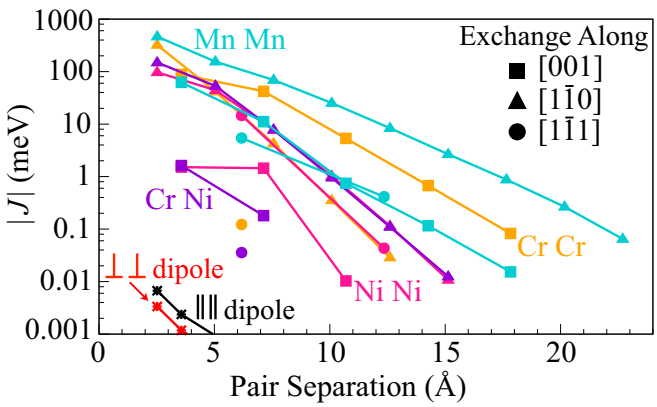

FIG. 3. Magnitude of the exchange interaction for several pairings of transition-metal spin centers along [001], [1$\bar{1}$0], and [1$\bar{1}$1], denoted by triangles, squares, and circles, respectively. The four sets of spin-center pairs are Mn-Mn (light blue), Ni-Ni (pink), Cr-Cr (gold), and Cr-Ni (purple).

is the largest for the Ni-Ni pair, and excluding the Ni-Ni pair, it is the direction for which the exchange interaction between other transition-metal pairs is the least. At pair spacings greater than ∼2 nm the energy broadening of the calculation (10 μeV) limits the ability to resolve the exchange splittings, and for several pairs of spin centers the exchange interaction is obscured at shorter distances by this broadening. At the first nearest-neighbor spacing in the [001] direction and the first- and second-nearest-neighbor spacing in the [1$\bar{1}$0] direction, the energy broadening in the calculation is on the order of 1 meV, and thus the error for these points is larger than the others. The exchange interaction is strongly anisotropic and can vary greatly depending on the direction of the interaction, the energy of the spin-center states, as well as the symmetry of the HOMO (which produces the greatest hybridization and splitting), i.e., e or t_2. For all these calculations the strength of the exchange interaction exceeds the dipolar interaction (also shown in Fig. 3) by orders of magnitude. Only for spin-center separations in excess of 3 nm would the dipolar interaction become comparable to the exchange interaction.

The NV^- center exhibits an additional form of exchange interaction anisotropy, corresponding to the dependence of the exchange interaction on the relative orientation of the NV^- center atoms themselves. The vacancy and the nitrogen can either be oriented near parallel to [1$\bar{1}$1] or near perpendicular to [1$\bar{1}$1]. This introduces four orientations for a pair of NV^- centers, (1) both near parallel to [1$\bar{1}$1], (2) both near perpendicular to [1$\bar{1}$1], and (3) and (4) corresponding to types with one of the pair near parallel and the other near perpendicular to [1$\bar{1}$1], pictured in Fig. 4. The choice of near-parallel or near-perpendicular orientation of the NV^- center has a large effect on the exchange interaction. Due to the geometry of NV^- center pairs along the [1$\bar{1}$0] direction, for some

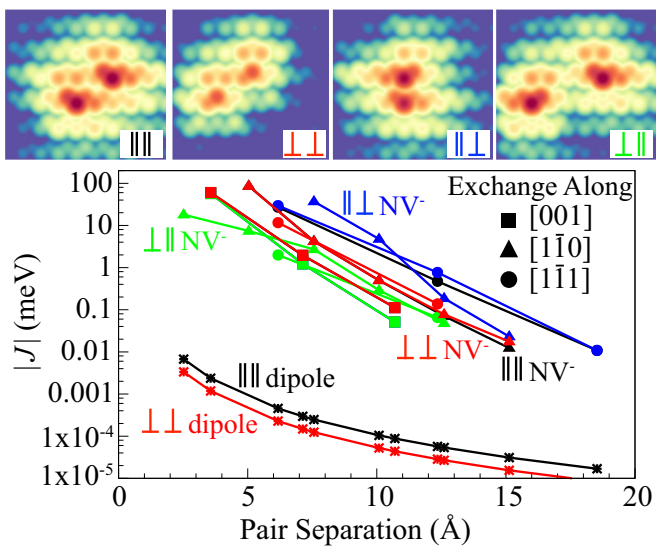

FIG. 4. Anisotropy of the exchange interaction for pairs of NV^- centers along [001], [1$\bar{1}$0], and [1$\bar{1}$1], denoted by triangles, squares, and circles, respectively. The insets are the four real-space probability densities representing the different orientations of the NV^- centers with respect to the [1$\bar{1}$1] direction. They are plotted in the (110) plane containing the centers, for two NV^- centers separated by 6.17 Å with the same logarithmic color scale used in Fig. 2.

pairs the first-nearest-neighbor and in one case the second-nearest-neighbor exchange interactions are not presented due to overlapping impurity potentials. As expected from the symmetry of the different pairs, in some directions there are pairs which have similar exchanges. For example, along the [001] direction, the exchange interactions between the near-parallel near-perpendicular (blue) and near-perpendicular near-parallel (green) pairs overlay each other in the plot as do the values for the near-perpendicular near-perpendicular (red) and near-parallel near-parallel (black) pairs. At the largest spacings, the near-parallel near-perpendicular (blue) and near-parallel near-parallel (black) pairs have the largest exchange interactions along $[1\bar{1}1]$, in direct contrast with the transition-metal pairs where the interactions along $[11\bar{1}]$ are in general the smallest. Once again, beyond these pair spacings the exchange interaction is hidden by the 10 μeV broadening included in the homogeneous Green's function calculations.

The exchange interactions between pairs of transition-metal pairs of spin centers and pairs of NV^- centers are comparable in magnitude. For all the species and orientations of pairs at the calculated separations the exchange interactions exceed the dipole-dipole interaction between two electrons, regardless of dipole orientation. Taking a linear fit to the logarithmic decrease of the exchange interaction along the $[1\bar{1}0]$ direction, as one would expect from the exponential decay of the localized dopant wave functions in space, the exchange interaction between two Mn equals the dipolar interaction at 47 Å; this crossover occurs at roughly 22 and 25 Å for the other transition-metal pairs and different orientations of NV^- pairs, respectively.

We have constructed a detailed and accurate theoretical description of NV^- and transition-metal point defect spin centers in diamond. The accuracy is due to the quality of the host band structure and the relative insensitivity of the exchange energy to the midgap state energies of the dopants. Once the host electronic propagators are tabulated, the calculation of the exchange energy proceeds in minutes on a current laptop computer. The exchange interactions for pairs of transition-metal spin centers are on the order, and in some cases, larger than the exchange interaction for pairs of NV^- centers. The spin-1 transition-metal dopants, Cr-Cr and Ni-Ni, show experimentally relevant exchange interactions, in excess of the dipolar interactions between spin centers, even at 2–3 nm separations. Sources of error in the exchange calculations include the broadening used in the calculations of the propagators, errors in the position of the midgap states from *ab initio* calculations, and errors in the host band structure. Transition-metal dopants in diamond offer distinct properties compared to NV^- spin centers due to the inclusion of d orbitals and the resulting spin-orbit interaction that permits high-speed electrical control of spin [25] and spin-sensitive optical selection rules. Additionally, based on the exchange between a Ni and Cr dopant pair, one could envision a quantum register where information is transferred to the spin of a Ni spin center and then that information is stored in the less accessible Cr spin. Effects such as Jahn-Teller distortions can also influence the exchange, perhaps quenching some part of the result obtained for the undistorted dopant.

We acknowledge support from an AFOSR MURI.

[1] P. M. Koenraad and M. E. Flatté, Nat. Mater. **10**, 91 (2011).
[2] A. J. Heinrich, J. A. Gupta, C. P. Lutz, and D. M. Eigler, Science **306**, 466 (2004).
[3] D. Kitchen, A. Richardella, J.-M. Tang, M. E. Flatté, and A. Yazdani, Nature (London) **442**, 436 (2006).
[4] D. M. Toyli, C. D. Weis, G. D. Fuchs, T. Schenkel, and D. D. Awschalom, Nano Lett. **10**, 3168 (2010).
[5] A. A. Khajetoorians, B. Chilian, J. Wiebe, S. Schuwalow, F. Lechermann, and R. Wiesendanger, Nature (London) **467**, 1084 (2010).
[6] D. H. Lee and J. A. Gupta, Science **330**, 1807 (2010).
[7] A. A. Khajetoorians, J. Wiebe, B. Chilian, and R. Wiesendanger, Science **332**, 1062 (2011).
[8] A. Spinelli, B. Bryant, F. Delgado, J. Fernández-Rossier, and A. F. Otte, Nat. Mater. **13**, 782 (2014).
[9] G. Balasubramanian, P. Neumann, D. Twitchen, M. Markham, R. Kolesov, N. Mizuochi, J. Isoya, J. Achard, J. Beck, J. Tissler, V. Jacques, P. R. Hemmer, F. Jelezko, and J. Wrachtrup, Nat. Mater. **8**, 383 (2009).
[10] K. Ohno, F. Joseph Heremans, L. C. Bassett, B. a. Myers, D. M. Toyli, A. C. Bleszynski Jayich, C. J. Palmstrøm, and D. D. Awschalom, Appl. Phys. Lett. **101**, 082413 (2012).
[11] B. A. Myers, A. Das, M. C. Dartiailh, K. Ohno, D. D. Awschalom, and A. C. Bleszynski Jayich, Phys. Rev. Lett. **113**, 027602 (2014).
[12] J. R. Rabeau, Y. L. Chin, S. Prawer, F. Jelezko, T. Gaebel, and J. Wrachtrup, Appl. Phys. Lett. **86**, 131926 (2005).
[13] I. Aharonovich, S. Castelletto, B. C. Johnson, J. C. McCallum, D. A. Simpson, A. D. Greentree, and S. Prawer, Phys. Rev. B **81**, 121201 (2010).
[14] F. Jelezko and J. Wrachtrup, Phys. Status Solidi A **203**, 3207 (2006).
[15] T. Chanier, C. E. Pryor, and M. E. Flatté, Europhys. Lett. **99**, 67006 (2012).
[16] T. Chanier, C. Pryor, and M. E. Flatté, Phys. Rev. B **86**, 085203 (2012).
[17] J. R. Weber, W. F. Koehl, J. B. Varley, A. Janotti, B. B. Buckley, C. G. Van de Walle, and D. D. Awschalom, Proc. Natl. Acad. Sci. USA **107**, 8513 (2010).
[18] M. W. Doherty, F. Dolde, H. Fedder, F. Jelezko, J. Wrachtrup, N. B. Manson, and L. C. L. Hollenberg, Phys. Rev. B **85**, 205203 (2012).
[19] J.-M. Jancu, R. Scholz, F. Beltram, and F. Bassani, Phys. Rev. B **57**, 6493 (1998).
[20] G. F. Koster and J. C. Slater, Phys. Rev. **95**, 1167 (1954).
[21] J.-M. Tang and M. E. Flatté, Phys. Rev. Lett. **92**, 047201 (2004).

[22] C. E. Moore, *Atomic Energy Levels as Derived From the Analyses of Optical Spectra* (National Bureau of Standards, Washington, D.C., 1949), Vol. I.

[23] C. E. Moore, *Atomic Energy Levels as Derived From the Analyses of Optical Spectra* (National Bureau of Standards, Washington, D.C., 1952), Vol. II.

[24] C. E. Moore, *Atomic Energy Levels as Derived From the Analyses of Optical Spectra* (National Bureau of Standards, Washington, D.C., 1958), Vol. III.

[25] J.-M. Tang, J. Levy, and M. E. Flatté, Phys. Rev. Lett. **97**, 106803 (2006).